On Capacity of Magnetic Induction-based Wireless Underground Sensor Networks

Zhi Sun and **Ian F. Akyildiz**

Broadband Wireless Networking Laboratory, School of Electrical and Computer Engineering

Georgia Institute of Technology, Atlanta, GA, 30332, United States

Email: {zsun; ian}@ece.gatech.edu

Abstract—The magnetic induction (MI)-based wireless underground sensor networks (WUSNs) use the novel MI waveguide technique to establish long range and low cost wireless communications in harsh underground environments, which enable a large variety of novel and important applications. One of the main research challenges is the theoretical study of the channel and network capacities in these networks. Compared to the traditional wireless networks, both the channel and network capacities of MI-based WUSNs have significant different characteristics due to the completely different signal propagation techniques and network geometric structure. Moreover, the usage of multiple resonant MI relay coils in MI-based WUSNs brings more reliability concerns. In this paper, mathematical models are developed to evaluate the channel capacity, network capacity, and the reliability of MI-based WUSNs. Specifically, the closed-form expression for the channel capacity in MI-based WUSNs is first derived to capture the effects of multiple system parameters. Then the network capacity scaling laws of MI-based WUSNs are investigated under different deployment strategies. Finally, the system reliability of MI-based WUSNs in terms of the channel capacity and network capacity is discussed. The results of this paper provide principles and guidelines for the design and deployment of MI-based WUSNs.

I. Introduction

By bringing the wireless sensor networks into the underground soil environment, the Wireless Underground Sensor Networks (WUSNs) enable a wide variety of novel and important applications, such as intelligent irrigation, mine disaster prevention and rescue, concealed border patrol, in-situ sensing for oil recovery, underground infrastructure monitoring, among others [1]. However, it is difficult to establish efficient wireless links among underground sensor nodes, since the traditional wireless communication techniques based on electromagnetic (EM) waves encounter two major problems in soil medium: 1) extremely small communication ranges (<5 m) due to high path loss, and 2) highly dynamic channel conditions caused by the time varying soil properties such as soil moisture [2].

The Magnetic Induction (MI)-based WUSNs use the novel MI waveguide technique [3], [4], [5] to establish efficient wireless communications in underground soil medium. As shown in Fig. 1, the underground sensor nodes in MI-based WUSNs are wirelessly connected by the MI waveguides consisting of multiple MI relay coils. The wireless communications are accomplished by the consecutive magnetic induction between adjacent MI relay coils. The MI waveguide technique is favorable in WUSNs due to the following five advantages.

- The communication range between two underground sensor nodes is up to 100 m. Hence, a fully connected network can be achieved without very high sensor density.
- The MI channel conditions remain constant in most soil medium since the attenuation rate of magnetic fields does not change in most types of transmission medium.
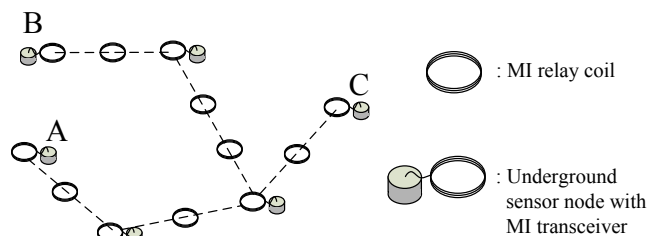

Fig. 1. The network geometric structure of the MI-based WUSNs.

- The MI relay coils do not consume extra energy and the unit cost is negligible.
- The relay coils are easy to deploy and do not need regular maintenances. The relay coils only need to be deployed every 6 to 12 m and can be flexibly deployed at any depth.
- The lifetime of MI-based WUSNs can be greatly prolonged since the underground sensor nodes equipped with MI transceivers can be recharged by aboveground devices using the inductive charging technique [6].

Despite the numerous advantages, the capacity and reliability of the MI-based WUSNs are the primary concerns. On the one hand, the bandwidth of the MI waveguide technique is much smaller than the terrestrial EM wave-based techniques since the MI relay coils have to work at the resonant frequency to maintain low path loss. Although the low duty circle WUSN applications do not require very high data rate, large scale WUSNs can still generate significant volume of traffic that needs to be efficiently delivered on the bandwidth limited MI channels via multi-hop wireless paths. Hence, a comprehensive analysis on the channel and network capacities of the MI-based WUSNs is necessary. On the other hand, since the communication success of the MI waveguide technique relies on multiple resonant MI relay coils, the functionality of the MI-based WUSNs depends on not only the underground sensor nodes but also all the MI relay coils. Therefore, the reliability of MI-based WUSNs needs to be examined in the harsh underground environments.

The theoretical study of the capacity and reliability in MI-based WUSNs is challenging and dramatically different from that of traditional wireless networks. First, due to the unique signal propagation solution, the bandwidth and received signal strength of the MI channel experience completely different attenuation law as the transmission distance increases. Consequently, the MI channel capacity has dramatically different characteristics from the traditional wireless channels. Second, since the MI signal can only propagate along the MI relay coils, the communication and interference ranges of a sensor node are no longer disks but can be arbitrary shapes depending

on the relay coil deployment strategy. For example, in Fig. 1, node A and a physically nearby node B can transmit at the same time without interference since they are far apart along the routes connected by the MI waveguides. However, A will be interfered by the simultaneous transmissions from a physically far away node C since they can close enough to each other thorough the relay coils. Hence, the network geometric structure of MI-based WUSNs in terms of connectivity and interference is significant different from traditional wireless networks. Due to the unique channel capacity and the network geometric structure, MI-based WUSNs also have dramatically different network capacity. Third, in MI-based WUSNs, not only sensor failure but also many other incidents, such as relay coil missing and displacement, can affect the system performance. Hence, the MI-based WUSNs encounter more severe reliability challenges than the traditional wireless networks. To our best knowledge, the above problems have not been addressed by the research community so far.

In this paper, we theoretically analyze the channel capacity, network capacity, and the reliability of the MI-based WUSNs. In particular, we first develop a mathematical expression of the channel capacity in WUSNs when the information propagation relies on the consecutive magnetic induction. The effects of multiple system parameters, including relay coil density, operating frequency, relay coil size, wire resistance, and number of turns of each relay coil, are captured. Based on the analysis of MI channel capacity, we investigate the network capacity scaling laws of MI-based WUSNs under different relay coil deployment strategies. The achievable throughput of each node is derived when the number of sensor nodes and the number of MI relay coils in the network increase. Finally, we discuss the impacts of different factors on the reliability of the channel capacity and the network capacity in MI-based WUSNs. The factors that we studied include the sensor node failure, relay coil missing, and direction and position deviation of the relay coils. The channel and network capacities as well as the corresponding reliabilities derived in this paper provide principles and guidelines for the design and deployment of MI-based WUSNs.

The remainder of this paper is organized as follows. In Section II, the related works are introduced. In Section III, the MI channel capacity between two underground sensor nodes is analyzed. In Section IV, the network capacity scaling laws of MI-based WUSNs are investigated under different deployment strategies based on the analysis of the MI channel capacity. Then, in Section V, the reliability of both the channel capacity and the network capacity in MI-based WUSNs is discussed. Finally, the paper is concluded in Section VI.

II. RELATED WORK

The definition of WUSNs is first proposed in [1]. We have developed the channel model of EM waves in soil medium in [2], which clearly shows the major problems of the EM wave-based techniques in WUSNs. This theoretical model has been validated by the testbed developed in [7]. In [8], we analyzed the connectivity of the WUSNs using EM waves. It is shown that an extremely high density of underground sensor nodes is required to form a fully connected network due to the small underground communication range.

In [3], we introduce the MI waveguide to WUSNs, which can greatly enlarge the underground communication range

without incurring very high cost. The MI waveguide technique is first developed in [4], [5]. It is shown that an array of loops can act as a waveguide, propagating a new form of wave known as a MI wave. The theoretical propagation model has been validated by experiments in [9]. The MI waveguide is originally designed as artificial delay lines and filters, dielectric mirrors, distributed Bragg reflectors, slow-wave structures in microwave tubes, coupled cavities in accelerators, and etc. In [3], we first utilize the MI waveguide in the field of wireless communications, where we adopt similar theoretical analysis method as [5]. In [10], we propose three strategies to deploy MI relay coils among unconnected underground sensor nodes to construct a fully connected network. The MI waveguide channel model in [3] and the MI waveguide deployment strategies in [10] provide the preliminary knowledge of the capacity and reliability analysis in this paper.

The capacity of traditional wireless networks using EM wave-based techniques has been intensively investigated by the research community. The network capacity scaling law of the traditional ad hoc networks is first studied in the seminal work [11]. The authors shows that the achievable throughput of each randomly located node decreases at the speed of $1/\sqrt{n \log n}$ as the number of nodes n in the network increase. In recent years, this seminal work has been extended to different types of wireless networks, such as the cognitive radio networks [12], the multi-channel multi-radio ad hoc networks [13], the ad hoc network with infrastructure [14], the ad hoc networks with MIMO or directional antenna [15], [16], among others. However, all the above works focus on the wireless networks that use traditional EM wave-based propagation techniques. None of the existing works considers a wireless network that has similar channel characteristics or network geometric structure as in the MI-based WUSNs. Moreover, there is no existing work considering the impacts of harsh environmental factors on the reliability of the channel and network capacities in MI-based WUSNs.

In this paper, we develop mathematical models to evaluate the channel and network capacities of MI-based WUSNs, which show dramatically different characteristics from those of the traditional wireless networks. Based on the capacity analysis, we investigate the influence of multiple system and environmental factors on the capacity reliability in MI-based WUSNs.

III. CHANNEL CAPACITY IN MI-BASED WUSNs

In this section, the capacity of the channel between two underground sensor nodes in the MI-based WUSNs is theoretically investigated. We start from the classic channel capacity formula given by:

$$C = B \cdot \log(1 + \frac{P_t \cdot L_p}{N}); \qquad (1)$$

where C is the channel capacity; B is the bandwidth of the channel; P_t is the transmission power; L_p is the path loss; and N is the total noise and interference power. In traditional EM wave-based wireless channel, the bandwidth B is a constant and previously determined by the specific applications; while the channel path loss L_p is an exponential function of the transmission distance. On the contrary, in MI-based WUSNs, the MI waveguide technique is used instead of the EM wave-based technique. Consequently, the bandwidth B is no longer

a constant but varies as the transmission distance increases or other system parameters change. Moreover, the path loss L_p of the MI waveguide is no longer a simple exponential function due to the consecutive magnetic induction. We have provide the channel model for the MI waveguide in soil medium in [3]. This channel model can be validated by the experiments conducted in [9]. In the following part of this section, we further develop this channel model to derive a close-form expression of the MI channel capacity, which lays the foundation of the network capacity analysis in next section.

A. Overview of the MI Waveguide Channel Model

Consider the MI channel between two sensor nodes that are d m apart from each other. The deployment density of MI relay coil is represented by the interval r between two adjacent relay coils, i.e. the relay coils are deployed every r m. Therefore, the MI waveguide consists of $k-1$ relay coils, $k = \lceil d/r \rceil$. If the frequency of the transmitting signal is f, the path loss of the MI waveguide can be calculated according to [3]:

$$L_p(d, r, f) \simeq 0.25 \left| \zeta(\tfrac{Z}{2\pi f M}, \lceil \tfrac{d}{r} \rceil) \right|^{-2} , \qquad (2)$$

where $\zeta(\tfrac{Z}{\omega M}, \lceil \tfrac{d}{r} \rceil)$ is the $\lceil \tfrac{d}{r} \rceil$ order polynomial of $\tfrac{Z}{\omega M}$; M is the mutual induction between the adjacent coils; and Z is the self impedance of one relay coil. The polynomial $\zeta(x, k)$ can be developed as

$$\zeta(x, 1) = x , \qquad (3)$$
$$\zeta(x, 2) = x^2 + 1 ,$$
$$\vdots$$
$$\zeta(x, k) = x \cdot \zeta(x, k-1) + \zeta(x, k-2).$$

The mutual induction M can be deduced by the magnetic potential of the magnetic dipole:

$$M \simeq \mu\pi N^2 \frac{a^4}{4r^3} \cdot (2\sin\theta_t \sin\theta_r + \cos\theta_t \cos\theta_r) \qquad (4)$$

where μ is the permeability of the soil medium; N is the number of turns of the wire on the coils; a is the radius of the coils; θ_t and θ_r are the angles between the coil radial directions and the line connecting the two coil centers.

B. Capacity of the MI Waveguide Channel

To derive the close-form formula of the MI channel capacity, the path loss and bandwidth of MI waveguide need to be explicitly expressed, where some approximation is required.

1) Closed-form Formula of the MI Waveguide Path Loss: The polynomial $\zeta(x, n)$ defined in (3) can be further developed as a closed form formula:

$$\zeta(x, k) = \frac{p^{2k} + (-1)^{k-1}}{p^{k-1} \cdot (p^2+1)} \cdot x + \frac{p^{2k-2} + (-1)^{k-2}}{p^{k-2} \cdot (p^2+1)} ; \qquad (5)$$

where $x = \tfrac{Z}{2\pi f M}$; $k = \lceil \tfrac{d}{r} \rceil$; p is a function of x given by

$$p = \frac{x + \sqrt{x^2 + 4}}{2} . \qquad (6)$$

In this paper, we let all the MI relay coils face up so that the coil axial direction is vertical ($\theta_t = \theta_r = 0$), as shown in Fig. 1. Although the planar coil deployment is not the direction that maximize the mutual induction, it guarantees that

each relay coil has omnidirectional communication range. The planar placed coils are also easy to deploy and stable during operations. Moreover, to maintain low path loss, in MI waveguide, the self impedance of a coil Z is designed to be resonant at the center frequency f_0 [3]. When $f = f_0$, Z becomes pure resistance R, which is the coil wire resistance. Consequently, if $\theta_t = \theta_r = 0$ and $f = f_0$, the variable x in the polynomial $\zeta(x, k)$ in (3) can be further developed as

$$x = \frac{Z}{2\pi f M} = \frac{2R \cdot r^3}{\mu\pi^2 f_0 N^2 a^4} . \qquad (7)$$

Since the self impedance of a coil Z is pure resistance R under the resonant status, the value of the polynomial $\zeta(x, n)$ becomes real. Then the path loss of the planar deployed MI waveguide working at the central frequency is given by

$$L_p(d, r, f_0) = 0.25\,\zeta^{-2}(\tfrac{2R \cdot r^3}{\mu\pi^2 f_0 N^2 a^4}, \lceil \tfrac{d}{r} \rceil) \qquad (8)$$
$$= 0.25 \left[\frac{p^{2\lceil \frac{d}{r} \rceil} + (-1)^{\lceil \frac{d}{r} \rceil -1}}{p^{\lceil \frac{d}{r} \rceil -1} \cdot (p^2+1)} \cdot x + \frac{p^{2\lceil \frac{d}{r} \rceil -2} + (-1)^{\lceil \frac{d}{r} \rceil -2}}{p^{\lceil \frac{d}{r} \rceil -2} \cdot (p^2+1)} \right]^{-2} ;$$

where x and p is defined in (7) and (6), respectively.

2) Closed-form Formula of the MI Waveguide Bandwidth: Since all the relay coils work at the resonant status, the bandwidth of the MI waveguide is very small and dramatically varies if the transmission distance or other parameters change. Recall that the self impedance of one relay coil $Z = R + j2\pi f L + \frac{1}{j2\pi f C}$, where R is the wire resistance; L is the self induction of each coil; and C is the loaded capacitor to guarantee resonance. The capacitor C is designed to fulfill $j2\pi f L + \frac{1}{j2\pi f C} = 0$ at the central frequency f_0. The self induction of each coil can be derived in the same way as the mutual induction. Hence, L and C can be calculated by

$$L \simeq \frac{1}{2}\mu\pi N^2 a ; \qquad C = \frac{2}{4\pi^2 f_0^2 N^2 \mu\pi a} . \qquad (9)$$

As the operating frequency deviates from the central frequency, the coil self impedance Z is no longer pure resistance and the absolute value dramatically increases. Consequently, the MI waveguide path loss also increases dramatically, which is the reason causing the small channel bandwidth. In this paper, we consider the 3-dB bandwidth B as the channel bandwidth. Specifically, the path loss at the frequency $f_0 + 0.5B$ is the two times as the path loss at the central frequency f_0, i.e. $L_p(d, r, f_0 + 0.5B) = 0.5 L_p(d, r, f_0)$. It should be noted that there may be multiple frequency where the path loss is doubled. In this case, the smallest B is the real 3-dB bandwidth. Substituting (2) into $L_p(d, r, f_0 + 0.5B) = 0.5 L_p(d, r, f_0)$ yields:

$$\frac{\left| \zeta(\frac{R + j2\pi(f_0 + 0.5B)L + \frac{1}{j2\pi(f_0 + 0.5B)C}}{2\pi f M}, \lceil \frac{d}{r} \rceil) \right|}{\zeta(\frac{R}{2\pi f_0 M}, \lceil \frac{d}{r} \rceil)} = \sqrt{2} , \qquad (10)$$

An equivalent approximation of (10) is needed to derive the closed form expression of the bandwidth. As previously mentioned, $\zeta(x, k)$ is the k order polynomial of x. Since $x = \frac{Z}{2\pi f M}$ is relatively large especially when the relay coil density is small (which is favorable for the deployment), the highest order variable in the polynomial has the most influence. Moreover, the bandwidth B is much smaller than the central frequency f_0. Therefore, (10) is approximately equivalent to the following
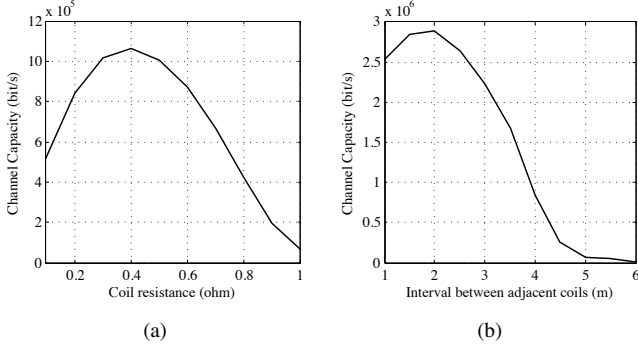
Fig. 2. The MI channel capacity as functions of (a) coil resistance and (b) coil interval length. (Note that the transmission distance is 40 m).
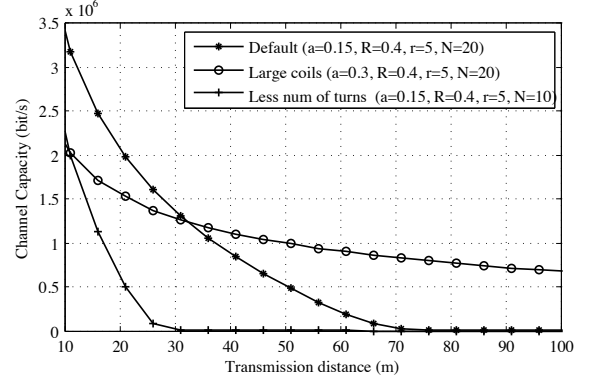

Fig. 3. The MI channel capacity as functions of the transmission distance with different MI waveguide parameters. (The coil resistance is set to the optimal value 0.4 Ω given in Fig. 2(a) while the coil interval is the maximum acceptable value 5 m)

equation:

$$\left| \frac{R + j2\pi(f_0+0.5B)L + \frac{1}{j2\pi(f_0+0.5B)C}}{R} \right|^{\lceil \frac{d}{r} \rceil} = \sqrt{2} , \quad (11)$$

By substituting (9) into (11), the closed form expression of the MI waveguide bandwidth can be approximately given by

$$B \simeq \frac{R}{\mu\pi^2 a} \sqrt{2^{\lceil \frac{d}{r} \rceil^{-1}} - 1} , \quad (12)$$

3) Closed-form Formula of the MI Waveguide Channel Capacity: Substituting (8) and (12) into (1) yields the closed-form formula of the MI waveguide channel capacity:

$$C \simeq \frac{R}{\mu\pi^2 a} \sqrt{2^{\lceil \frac{d}{r} \rceil^{-1}} - 1} \cdot \log \left[1 + \frac{P_t \cdot \zeta^{-2}(\frac{2R \cdot r^3}{\mu\pi^2 f_0 N^2 a^4}, \lceil \frac{d}{r} \rceil)}{4N} \right]; \quad (13)$$

C. Numerical Analysis

The channel capacity in MI-based WUSNs is numerically analyzed with different system configurations in this subsection. The default values are set as follows. The transmission power is set to be 10 *mW* (10 *dBm*). The operating frequency is 10 MHz. The relay coils have the same radius of 0.15 m and the number of turns is 20. The background noise level is −105 *dBm*. The permeability of the underground soil medium is a constant and is similar to the permeability of the air, since most soil in the nature does not contain magnetite. Therefore, $\mu = 4\pi \times 10^{-7}$ H/m. The soil moisture as well as other soil properties do not affect the MI communication as discussed perviously.

In Fig. 2, the channel capacities of MI waveguides with different coil resistance R and coil interval length r are provided. Tradeoffs exist here, since reducing coil resistance can reduce the path loss but also reduce the bandwidth, while the increasing the interval length between adjacent coils can increase the bandwidth but also increase the path loss. Hence, there exist optimal coil resistance and relay coil density to maximize the channel capacity, as shown in Fig. 2. It should be noted that although the coil resistance can be freely set to the optimal value, the coil interval is usually set as large as possible to reduce the number of relay coils.

Fig. 3 shows the channel capacities of MI waveguides as a function of transmission distance. The effects of different coil sizes and number of turns (as well as the operating frequency) are also captured. Different from the traditional

wireless channels, both the SNR and the bandwidth dramatically decreases as the transmission distance increases. Hence, the channel capacity attenuates very fast (Mbps in 20 m v.s. kbps in 70 m). This fast attenuation cannot be compensated by just increasing the transmission power since the power has no influence on the bandwidth. Increasing coil size can slightly reduce the bandwidth but can also dramatically reduce the path loss, especially in long distance transmission. Therefore, the channel capacity with larger coil size is lower in the near region but attenuates much slower. Increasing either operating frequency or the number of turns of each coil can increase the mutual induction; hence, they have the same effects on the channel capacity.

IV. NETWORK CAPACITY IN MI-BASED WUSNs

After deriving the channel capacity between a pair of underground sensors, we investigate the achievable throughput of each node, which serves as a lower bound of the network capacity in MI-based WUSNs. Since both the maximum link data rate (channel capacity) and the network geometric structure of the MI-based WUSNs is dramatically different from the traditional wireless networks, the network capacity also have significant different characteristics. The network geometric structure of the MI-based WUSNs is determined by the positions where the MI relay coils are deployed. Therefore, the network capacity is influenced by the MI waveguide deployment strategies. In [10], we have proposed three types of MI waveguide deployment strategies to construct fully connected WUSNs. In this section, we analyze the network capacity of the MI-based WUSNs constructed by the three types of deployment strategies.

A. Network Model and Deployment Strategies

In this paper, we consider a large scale WUSN with n underground sensor nodes $\{X_1, X_2, ...X_n\}$ randomly located in a disk of area S m^2 in the plane. Each node, equipped with a MI transceiver coil, is independently and uniformly distributed in the field. MI relay coils are deployed among the underground sensor nodes to relay magnetic induction signal between adjacent sensor nodes, as shown in Fig. 1. Each underground sensor node acts as a source node and has a randomly and independently chosen destination node. Our goal is to find the mathematical expression of the achievable throughput of each node $\lambda(n)$. The achievable throughput of
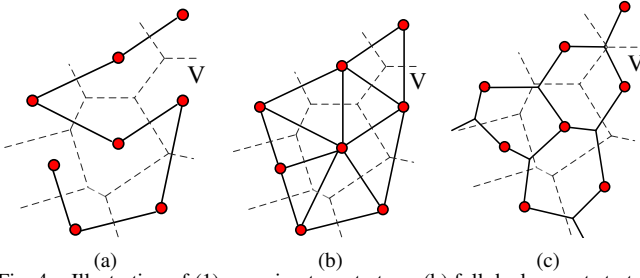
Fig. 4. Illustration of (1) spanning tree strategy, (b) full deployment strategy, and (c) triangle centroid strategy (Dots represent underground sensor nodes; solid lines represent MI waveguide; dashed lines are Voronoi tessellations V).

each node $\lambda(n)$ is defined as the maximum data rate that can be sent from each source to its destination in a multi-hop fashion under a spatial and temporal transmission scheduling scheme. Since the underground sensor nodes are low cost device with limit processing ability, we assume that all transmissions employ the same power $P_t(n)$, where $P_t(n)$ can be adjusted before the WUSN deployment to guarantee a certain level of communication range $d(n)$. Each node can transmit at $C(n)$ bits per second over a common MI channel. In this paper, to maximize the achievable throughput, we use the channel capacity derived in the previous section as $C(n)$. We define that the minimum signal-to-interference-plus-noise ratio (SINR) for successful communication under the data rate $C(n)$ is β. Hence, a transmission between transmitter X_i and receiver X_j is successful if and only if

$$\frac{P_t(n) \cdot 0.25\, \zeta^{-2}(x, \lceil \frac{|X_i - X_j|}{r} \rceil)}{N_0 + \sum_{k \neq i} P_t(n) \cdot 0.25\, \zeta^{-2}(x, \lceil \frac{|X_k - X_j|}{r} \rceil)} \geq \beta\,; \qquad (14)$$

where x is given by (7); N_0 is the Gaussian noise power; and the sum in the denominator is the total interference from all simultaneously transmissions.

Then the maximum transmission rate $C(n)$ can be given by

$$C(n) = \frac{R}{\mu \pi^2 a} \sqrt{2^{\lceil \frac{d(n)}{r} \rceil - 1} - 1} \cdot \log(1 + \beta)\,; \qquad (15)$$

To facilitate the analysis, we also defined an interference range $D(n)$. Two transmitters can transmit simultaneously without interfering each other if they are $D(n)$ apart. The relationship between the communication range $d(n)$ and the interference range $D(n)$ is determined by the MI relay coil deployment strategy and is discussed in the following subsections.

We consider three important strategies to deploy the MI relay coils to construct a fully connected WUSNs [10]:

- *The spanning tree strategy:* As shown in Fig. 4(a), the Voronoi tessellation of the sensor nodes (denoted as V) partitions the whole field into Voronoi cells. A spanning tree is constructed by using all sensors as vertexes and all links connecting sensors in adjacent Voronoi cells in V as edges. By deploying MI relay coils along all the edges in the spanning tree, the whole WUSN is fully connected. The spanning tree strategy strategy use minimum number of relay coils but is not robust to sensor node failures.
- *The full deployment strategy:* As shown in Fig. 4(b), the MI waveguides are deployed along all the edges that connecting sensors in adjacent Voronoi cells in V. The full deployment strategy consumes more relay coils but
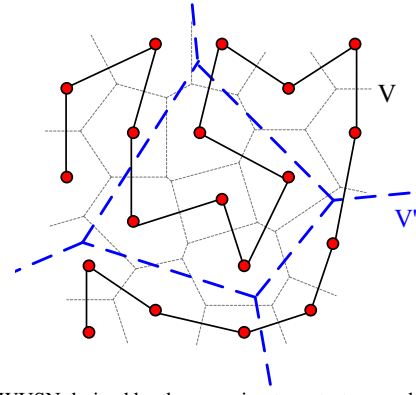

Fig. 5. The WUSN derived by the spanning tree strategy and two independent Voronoi tessellations V and V' constructed on such WUSN.

is robust to sensor node failures.
- *The triangle centroid strategy:* By connecting the nodes that are in adjacent Voronoi cells in V, the whole field is partitioned into non-overlapped triangle cells. In every other triangle cell, the MI waveguide is deployed along the three-pointed star centered at the triangle centroid, as shown in Fig. 4(c). The triangle centroid strategy achieves the same robustness to sensor node failures as the full deployment but consumes much less MI relay coils [10].

The full deployment strategy and the triangle centroid strategy can construct a WUSN with almost the same geometric structures while the WUSN derived by the spanning tree strategy has a completely different network geometric structure. Hence, in the following two subsections, we investigate the network capacity of MI-based WUSNs under the two network geometric structures: the structure created by the spanning tree strategy and the structure created by the full deployment/triangle centroid strategy. It should be noted that we assume the density of the MI relay coils remains the same while the number of underground sensor nodes scales. In another word, as the sensor node density increases, the number of relay coils between two sensor nodes decreases since the interval between adjacent relay coils r remains same. The area S of the disk shaped field is large enough so that the intermediate distances between adjacent underground sensor nodes are much longer than r.

B. Network Capacity Scaling Law of WUSN Constructed by the Spanning Tree Strategy

1) Communication Range $d(n)$ and the Resulted Network Geometric Structure: According to [11], the whole field can be also be divided by a new Voronoi tessellation (denoted as V'), where each Voronoi cell contains a disk of radius $\sqrt{\frac{100 S \log n}{\pi n}}$ and is contained in a disk of radius $2\sqrt{\frac{100 S \log n}{\pi n}}$. It has been proved in [11] that each cell in the new Voronoi tessellation V' contains at least one underground sensor node.

After deriving V' (dashed lines in Fig. 5), the spanning tree strategy can be applied in such WUSN to deploy MI waveguides. It is not difficult to find a spanning tree with only two leaves (i.e. a path graph, denoted as G_p) connecting all underground sensors in V while the path of the spanning tree passes each Voronoi cell in V' just once, as shown in Fig. 5.

The maximum distance between any points in adjacent Voronoi cells in V' is $8\sqrt{\frac{100 S \log n}{\pi n}}$. Therefore, if the trans-

mission range of the underground sensor node is $d(n) = 8\sqrt{\frac{100S\log n}{\pi n}}$, it is guaranteed that there is at least one sensor node in one Voronoi cells in V' can communicate with another sensor node in the two adjacent Voronoi cell that is connected by the path graph G_p. By this means, a fully connected WUSN is derived and has a linear geometric structure. It should be noted that a sensor node in a Voronoi cell in V' can only communicate with (or interfere) another Voronoi cell through the path graph G_p where the MI relay coils are deployed.

2) Interference Range $D(n)$ and the Upper Bound of Cell Interfering Neighbor Number:

Lemma 1: The interference range $D(n)$ under the spanning tree deployment strategy is:

$$D(n) = r\log_x(2\beta) + 2d(n);\qquad(16)$$

where $d(n) = 8\sqrt{\frac{100S\log n}{\pi n}}$ is the communication range; r is the fixed interval length between two adjacent relay coils; and x is given in (7)

Proof: Since the interference range is $D(n)$, the disks of radius $0.5D(n)$ around each simultaneously transmitting node are disjoint. In other word, on the path graph G_p, every simultaneously transmitting node is $D(n)$ apart from each other. Then the SIR at a receiver X_j is lower bounded by

$$\frac{P_t(n)\cdot 0.25\cdot \zeta^{-2}(x,\lceil\frac{d(n)}{r}\rceil)}{N_0 + \sum_{k=1}^{+\infty}2\cdot P_t(n)\cdot 0.25\cdot \zeta^{-2}(x,\lceil\frac{0.5kD(n)}{r}\rceil)} \qquad(17)$$
$$= \frac{\frac{P_t(n)}{N_0}}{4\zeta^2(x,\lceil\frac{d(n)}{r}\rceil) + 2\frac{P_t(n)}{N_0}\cdot\sum_{k=1}^{+\infty}\left[\frac{\zeta(x,\lceil\frac{d(n)}{r}\rceil)}{\zeta(x,\lceil\frac{0.5kD(n)}{r}\rceil)}\right]^2};$$

Note that the coefficient 2 in the denominator is added since there may exist two simultaneous transmitter on each side of the current transmitter on path graph G_p. In the sum in the denominator in (17), each addend is a fraction. According to the definition of $\zeta(x,k)$ given in (3), the denominator $\zeta(x,\lceil\frac{0.5kD(n)}{r}\rceil)$ is in fact a weighted sum of the numerator $\zeta(x,\lceil\frac{d(n)}{r}\rceil)$, where the weights consists of $\{1,x,x^2,...,x^{\lceil\frac{0.5kD(n)}{r}\rceil-\lceil\frac{d(n)}{r}\rceil}\}$. Similar to the analysis in Section III, since x is relatively large, the highest order variable of x has the most influence. Therefore, the fraction in the sum in (17) can be upper bounded by:

$$\frac{\zeta(x,\lceil\frac{d(n)}{r}\rceil)}{\zeta(x,\lceil\frac{0.5kD(n)}{r}\rceil)} < x^{-\left(\lceil\frac{0.5kD(n)}{r}\rceil-\lceil\frac{d(n)}{r}\rceil\right)}\qquad(18)$$

Since the transmission power $P_t(n) >> N_0$, the SIR at a receiver X_j is approximately lower bounded by the following value that should be larger than the threshold β:

$$\frac{1}{2\sum_{k=1}^{+\infty}x^{-2\left(\lceil\frac{0.5kD(n)}{r}\rceil-\lceil\frac{d(n)}{r}\rceil\right)}} \geq \beta;\qquad(19)$$

Therefore the safe interference range $D(n)$ to derive the required SIR is

$$D(n) = \frac{r}{\log x}\log(1 + 2\beta\cdot x^{2\lceil\frac{d(n)}{r}\rceil}) \simeq r\log_x(2\beta) + 2d(n);\quad(20)$$

∎

We define a Voronoi cell in V' is an interfering neighbor of another cell if the minimum distance between the two cells along the path graph G_p is smaller than the interference range $D(n)$.

Lemma 2: Every cell in V' has no more than $44 + \frac{16r\log_x(2\beta)}{d(n)}$ interfering neighbor cells.

Proof: The Voronoi cells can only interfere each other through the MI waveguides on the path graph G_p. Hence, it only needs to calculate how many Voronoi cells can be accommodated along the path graph G_p within the interference range. All the Voronoi cells in V' are contained by a disk of radius $\frac{1}{4}d(n)$ and the interference range is $D(n)$, all interfering neighbor cells have to be within a line segment of length $2*[3*\frac{1}{4}d(n)+D(n)]$. Additionally, since each cell in V' contains a disk of radius $\frac{1}{8}d(n)$, the line segment cannot cross more than $\frac{2*[3*\frac{1}{4}d(n)+D(n)]}{\frac{1}{8}d(n)}$ cells in V', which completes the proof. ∎

3) Spatial and Temporal Transmission Schedule: After deriving the upper bound of the number of interfering neighbors, a temporal transmission schedule can be designed to guarantee the success of each transmission. Specifically, each duty cycle is divided into $45 + \frac{16r\log_x(2\beta)}{d(n)}$ slots and each Voronoi cell in V' gets one slot to transmit data. Since all the Voronoi cells are along the path graph G_p, we just need to periodically allocate the $45 + \frac{16r\log_x(2\beta)}{d(n)}$ slots to the Voronoi cells in V' along the path graph G_p in serial order. Since the maximum number of interfering neighbor cells is $45 + \frac{16r\log_x(2\beta)}{d(n)}$, the sensor node in every cell can successfully received the data from a transmitter within the distance $d(n)$ by using the above transmission schedule.

Since each Voronoi cell in V' contains at least one underground sensor node and the sensor nodes in each cell are guaranteed to be able to communicate with the adjacent sensor nodes along the path graph G_p, for any source-destination pair, there exists a route along the path graph G_p that connects the source node and the destination node.

4) The Mean Number and the Actual Number of the Routes Served by Each Cell: Before deriving the network capacity, the traffic load of each Voronoi cell in V' needs to be investigated first. We consider the route R_{sd} from the source X_s to the destination X_d and check .

Lemma 3: The probability that the route R_{sd} intersects any one Voronoi cell v in V' is upper bounded by

$$P(R_{sd}\text{ intersects }v) \leq \frac{1}{2} + \frac{c_0\log n}{n}\qquad(21)$$

where c_0 is a constant.

Proof: As discussed previously, all underground sensor nodes are along a path graph G_p. We can sequentially denote those node as $\{X_i, i = 1,...,n\}$ along the path. The source node X_s and the destination node X_d are among the ordered sensor nodes. Assuming that the Voronoi cell v contains the mth sensor nodes X_m. Due to the linear network structure, R_{sd} intersects v if and only if X_m is in the middle of X_s and X_d on the path graph. Since source X_s and destination X_d are uniformly selected from $\{X_i, i = 1,...,n\}$,

$$P(R_{sd}\text{ intersects }X_m)$$
$$= P(s < m)\cdot P(d > m) + P(s > m)\cdot P(d < m)$$
$$= 2\frac{m-1}{n}\frac{n-m}{n}.\qquad(22)$$

$P(R_{sd}$ intersects $X_m)$ in (22) achieves the maximum value if $m = \lceil \frac{n}{2} \rceil$. Note that one Voronoi cell in V' may contain multiple sensor nodes. The number of nodes in each cell is lower bounded by $c_l \log n$ and upper bounded by $c_u \log n$, according to [11]. Then

$$P(R_{sd} \text{ intersects } v)$$
$$< \max\{P(R_{sd} \text{ intersects } X_m)\} + 2P(X_i \text{ is inside } v)$$
$$\leq \frac{1}{2} + 2\frac{c_u \log n}{n} ; \tag{23}$$

This completes the proof. ∎

Since the number of total routes is n (every node acts as as source and one route for one source-destination pair), the mean number of the routes served by each cell is

$$E[\text{Number of routes intersecting } v] < \frac{n}{2} + c_0 \log n . \tag{24}$$

Next, we use the Vapnik-Chervonenkis Theorem, similar strategy as in [11], to prove that the actual number of routes intersecting a cell converges to the above derived mean value. The proof procedure is similar to the method in [11], hence, is omitted here. Then, we have

Lemma 4: There exists a $\delta(n) \to 0$ as $n \to \infty$ such that

$$P\left[\sup_{v \in V'}(\text{Number of routes intersecting } v) \leq \frac{n}{2} + c_0 \log n\right]$$
$$\geq 1 - \delta(n) . \tag{25}$$

5) Achievable Throughput of Each Node under the Spanning Tree Strategy: By using the transmission schedule scheme given previously, each Voronoi cell in V' can successfully transmit data in the allocated time slot. Since the channel capacity is $C(n)$ given by (15), the data rate each cell can use is the channel capacity $C(n)$ divided by the total number of time slots $45 + \frac{16r \log_x(2\beta)}{d(n)}$. Meanwhile, the traffic load for each Voronoi cell in V' is given by the throughput of each node $\lambda(n)$ multiplied by the actual number of routes served by each cell. In the most efficient case, the traffic load per cell is equal to the available data rate. Hence, we have

$$\lambda(n) \cdot \left(\frac{n}{2} + c_0 \log n\right) = \frac{C(n)}{45 + \frac{16r \log_x(2\beta)}{d(n)}} . \tag{26}$$

Then the achievable throughput of each underground sensor node under the spanning tree strategy in MI-based WUSNs is derived.

Theorem 1: For MI-based WUSN constructed by the spanning tree strategy, the achievable throughput of each underground sensor node is:

$$\lambda(n) = \frac{2}{n + 2c_0 \log n} \cdot \frac{R}{\mu \pi^2 a} \sqrt{2^{\lceil \frac{d(n)}{r} \rceil - 1} - 1} \cdot \frac{\log(1 + \beta)}{45 + \frac{16r \log_x(2\beta)}{d(n)}}$$
$$\simeq c_1 \cdot \frac{1}{n + 2c_0 \log n} \cdot \left(2^{c_2 \sqrt{n/\log n}} - 1\right)^{\frac{1}{2}} . \tag{27}$$

where c_1 and c_2 only depend on the SIR threshold β and the MI waveguide parameters but do not depends on the sensor node number n.

Compared with the achievable throughput in traditional wireless networks ($\frac{c}{\sqrt{n \log n}}$) [11], we can find dramatical differences in the throughput of MI-based WUSNs in (27).

C. Network Capacity Scaling Law of WUSN Constructed by the Full Deployment Strategy and Triangle Centroid Strategy

The WUSN constructed by the full deployment strategy or the triangle centroid strategy has completely different network geometric structure than that of the spanning tree strategy. As a result, the achievable network capacities of the former two deployment strategies are also different.

As shown in Fig. 4(b) and Fig. 4(c), in full deployment strategy and the triangle centroid strategy, the MI relay coils are deployed to connect all the underground sensors in adjacent Voronoi cells in V. The only different is the route of the MI waveguide: the triangle centroid strategy places the MI waveguide along the three-pointed star in every other cell; while the full deployment strategy places the relay coils along all the edges of the triangle cells. However, the network connectivity and topology are exactly the same for these two deployment strategies. Hence, they share the same network capacity scaling law.

Since each underground sensor nodes can directly communicate with all its adjacent sensor nodes, the communication and interference range of such sensor nodes are almost isotropic, which yields the network geometric structure just like the traditional wireless networks. Therefore, the results derived in [11] can be unitized but needs modifications. Due to the usage of the MI waveguide, the channel capacity and the interference model is different from the traditional wireless networks. Therefore the network capacity of such WUSNs can be derived by using similar strategies in Section IV-B and the results in [11].

Theorem 2: For MI-based WUSN constructed by the full deployment strategy or the triangle centroid strategy, the achievable throughput of each underground sensor node is:

$$\lambda(n) \simeq \frac{c_3}{\sqrt{n \log n}} \cdot \left(2^{c_2 \sqrt{n/\log n}} - 1\right)^{\frac{1}{2}} . \tag{28}$$

where c_2 and c_3 are variables only depending on the SIR threshold β and the MI waveguide parameters.

Compared (28) with the achievable throughput in traditional wireless networks and in WUSNs constructed by the spanning tree strategy, we can find the throughput of MI-based WUSNs in (28) decreases significantly slower than (27) and the ($\frac{c}{\sqrt{n \log n}}$) in [11].

D. Numerical Analysis

In Fig. 6, the network capacity scaling laws of the traditional Ad hoc networks and the MI-based WUSNs are compared. For fairness, the normalized achievable throughput $\overline{\lambda(n)} = \lambda(n)/\lambda(n_0)$ is plotted, which can eliminate the effects of constants that do not depends on the node number n. It should be noted that the scaling laws of the MI-based WUSNs is a function of the variable $c_2 \sqrt{n/\log n}$ in (27) and (28), which is determined by $d(n)$ and r. The constant c_2 needs to be selected before the numerical comparison. Since we assume that intermediate distances between adjacent underground sensor nodes should be longer than the coil interval r, c_2 can be selected accordingly. In Fig. 6, we let $c_2 = \sqrt{\frac{\log 1000}{1000}}$. Fig. 6 shows that the network capacity of WUSNs constructed by the spanning tree strategy has similar decreasing speed as the traditional Ad hoc networks as the node number increases, which is the
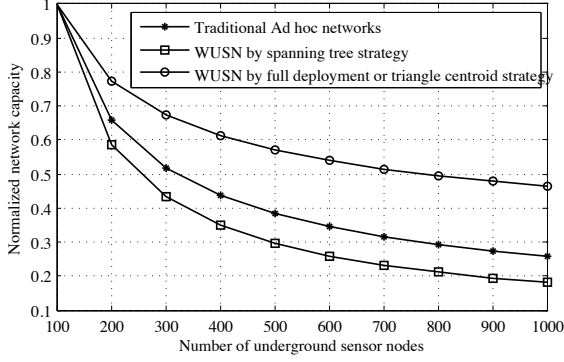
Fig. 6. The network capacity scaling laws of the traditional Ad hoc networks, the MI-based WUSNs constructed by the spanning tree strategy, and the the MI-based WUSNs constructed by the full deployment or triangle centroid strategy.

joint effect of two factors: the $\frac{1}{n+2c_0 \log n}$ in (27) drops much faster than the $\frac{1}{\sqrt{n \log n}}$ of traditional networks; however, the $(2^{c_2 \sqrt{n/\log n}} - 1)^{\frac{1}{2}}$ in (27) can dramatically compensate this fast attenuation. Fig. 6 also indicates that the network capacity of WUSNs constructed by the full deployment or the triangle centroid strategy falls much slower than the traditional Ad hoc networks as the node number increases due to the following reason. Although these two types of networks have almost the same geometric structure, the network capacity of the MI-based WUSNs can benefit from the increased node density since the MI channel bandwidth increases dramatically as the node intermediate distance decreases.

V. Discussion on the Reliability of the Channel and Network Capacities in MI-based WUSNs

In this section, we investigate the impacts of several factors on the channel and network capacities in MI-based WUSNs derived in the previous two sections. The factors that we studied include the sensor node failure, relay coil missing, and direction/position deviation of the relay coils. The influence of these factors on the channel and network capacities reflects the system reliability of the MI-based WUSNs under different deployment strategies.

A. Unreliability due to Node Failure

In harsh underground environments, sensor node failure may frequently happen due to device damage, malfunction, or dead battery. The sensor node failure cannot affect the channel capacity of the remaining links. However, node failure can change the network geometric structure. Hence the network capacity can be influenced by the node failure.

The network capacities of WUSNs constructed by different MI waveguide deployment strategies have different robustness to node failure.

- In WUSNs constructed by the spanning tree strategy, the failure of any one node will partition the whole network into two disconnected networks. According to (24), by deleting one node, up to half of the routes are disconnected. As a result, up to 50% of traffic load cannot be delivered since there is only one route connecting each source-destination pair. Consequently, if only one sensor node fails, the achievable network capacity can drop to as low as 50% of the original value. Therefore, the

node failure can significantly affect the reliability of the network capacity of the MI-based WUSNs constructed by the spanning tree strategy.

- In WUSNs constructed by the full deployment strategy or triangle centroid strategy, each sensor node is connected to all its adjacent neighbors. The failure of a few sensor nodes cannot partition the network into unconnected parts. If the remaining source and destination nodes are aware of the failure of any node in the network, it is not difficult to find other near routes to avoid the failed sensor nodes. This may slightly rise the traffic load of nearby sensor nodes. However, consider the large number of sensor nodes in the investigated large scale network, the change of the average achievable throughput of each node can be neglected. Therefore, the node failure has little influence on the reliability of the network capacity of the MI-based WUSNs constructed by the full deployment strategy or triangle centroid strategy.

B. Unreliability due to Relay Coil Missing and Direction/Position Deviation

As discussed previously, the MI waveguides consists of multiple MI relay coils. The channel model in Section III assumes that all relay coils are placed at the designed position at right angle. However, in the practical operation, this assumption may not hold since: 1) the relay coils may be damaged by the harsh underground environments; and 2) the position and direction of each relay coils may deviate due to the environmental perturbations.

The relay coil missing and direction/position deviation cannot disconnect a wireless link immediately. Hence, those factors cannot change the network geometric structure. However, the unreliability caused by the relay coils can gradually reduce the channel capacity and consequently affect the network capacity. In the following, we re-exam the channel capacity under the influence of the relay coil missing, the position deviation, and the direction deviation.

Due to the above three factors, the mutual induction defined in (4) between each pair of adjacent relay coils $\{M_i, i = 1, 2, ...n\}$ is no longer the same. In particular, the missing of a certain relay coil can cause a certain coil interval doubled and the total relay number $\lceil \frac{d}{r} \rceil$ decreased by 1. The coil position deviation will cause the fluctuations of the coil interval r along the MI waveguide. The coil direction deviation may cause the θ_t and θ_r become a value other than $0°$. Moreover, since the mutual inductions $\{M_i, i = 1, 2, ...n\}$ are no longer the same, the path loss in (2) needs to be modified as

$$L'_p(k, f) \simeq 0.25 \cdot \left[(2\pi f)^k \cdot \prod_{i=1}^{k} M_i \right]^2 \cdot |\zeta'_k|^{-2}, \quad (29)$$

where $k - 1$ is the number of functional relay coils between the two underground sensors; the polynomial ζ'_k is defined as

$$\zeta'_1 = Z, \quad (30)$$
$$\zeta'_2 = Z^2 + 4\pi^2 f_0^2 M_1^2,$$
$$\vdots$$
$$\zeta'_k = Z \cdot \zeta'_{k-1} + 4\pi^2 f_0^2 M_{k-1}^2 \cdot \zeta'_{k-2}.$$

Once the new path loss is derived, the new 3-dB bandwidth B' can be calculated by letting the path loss at the frequency $f_0 +$
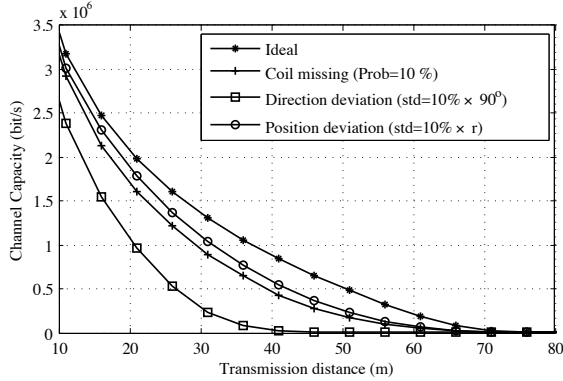
Fig. 7. The channel capacity of MI-based WUSNs under the impacts of coil missing, direction deviation, and position deviation.

$0.5B$ is the two times as the path loss at the central frequency f_0, i.e. $L'_p(k, f_0 + 0.5B') = 0.5L'_p(k, f_0)$.

Due to the randomness of the coil missing and the direction/position deviation, it is impossible to derive the close-form expression of the channel capacity under those factors. In the following, we conduct numerical evaluations on the impacts of relay coil missing and direction/position deviation. It should be noted that the impact of those factors on the channel capacity is proportional to the impact on the network capacity, since neither the coil missing nor the direction/position deviation can change the network geometric structure. Therefore, we focus on the impact on the channel capacity.

Using the same default parameters given in Section III, we consider three scenarios: 1) each relay coil has a probability of 10% to be damaged and cannot function; 2) the direction of each relay coil θ deviate from $0°$ by x_d, where x_d is zero mean gaussian variable with a standard deviation $10\% \times 90°$; and 3) the position of each relay coil deviate from the original position by x_p, where x_p is zero mean gaussian variable with a standard deviation $10\% \times r$. The results shown in Fig. 7 are the average of 100 iterations. Fig. 7 shows that the coil direction deviation has the most severe impacts on the channel capacity (as well as the network capacity) of the MI-based WUSNs since the consecutive magnetic inductions depend on the proper direction of all relay coils. Meanwhile the impacts of the position deviation are not significant since it only causes mild fluctuations of the mutual inductions. The impacts caused by the lost a small number of relay coils are in between the impacts of the above two factors.

VI. CONCLUSIONS

Due to the different signal propagation technique and network geometric structure, the MI-based WUSNs have dramatically different channel and network capacities. The investigation of the channel and network capacities as well as their reliabilities in MI-based WUSNs is essential for the WUSN design due to the extremely limited bandwidth and the impacts of harsh operation environments. In this paper, we provide close-form expressions for the channel capacity and the achievable network capacity of the MI-based WUSNs under three types of MI waveguide deployment strategies. The reliability of the channel and network capacities is also investigated under the impacts of sensor node failure and MI relay coil missing and displacement. Our analysis shows that

the channel capacity attenuates very fast as the transmission distance increases and is influenced by multiple coil parameters. The very limited channel capacity is due to the resonant working status and cannot be effectively enlarged by simply increasing the transmission power. Compared with the scaling law of $\frac{c}{\sqrt{n \log n}}$ in traditional wireless networks, the network capacity of the MI-based WUSNs has dramatically different scaling laws: the WUSNs constructed by the spanning tree deployment strategy have the network capacity scaling law of $\frac{c_1}{n + c_0 \log n} \cdot (2^{c_2 \sqrt{n/\log n}} - 1)^{\frac{1}{2}}$, which is very sensitive to sensor node failures; while the WUSNs constructed by full deployment or triangle centroid strategy have the scaling law of $\frac{c_3}{\sqrt{n \log n}} \cdot (2^{c_2 \sqrt{n/\log n}} - 1)^{\frac{1}{2}}$, which is much more robust to sensor node failures.

REFERENCES

[1] I. F. Akyildiz and E. P. Stuntebeck, "Wireless underground sensor networks: Research challenges," *Ad Hoc Networks Journal (Elsevier)*, vol. 4, pp. 669-686, July 2006.
[2] I. F. Akyildiz, Z. Sun, and M. C. Vuran, "Signal Propagation Techniques for Wireless Underground Communication Networks," *Physical Communication Journal (Elsevier)*, vol. 2, no. 3, pp.167-183, September 2009.
[3] Z. Sun and I. F. Akyildiz, "Magnetic Induction Communications for Wireless Underground Sensor Networks," *IEEE Transactions on Antennas and Propagation*, vol. 58, no. 7, pp. 2426-2435, July 2010.
[4] R. R. A Syms, I. R. Young and L. Solymar, "Low-loss magneto-inductive waveguides," *Journal of Physics D: Applied Physics*, vol. 39, pp. 3945-3951, 2006.
[5] V. A. Kalinin, K.H. Ringhofer; L. Solymar, "Magneto-inductive waves in one, two, and three dimensions," *Journal of Applied Physics*, vol. 92, no. 10, pp. 6252-6261, 2002.
[6] A. Karalis, J.D. Joannopoulos, and M. Soljacic, "Efficient Wireless Non-Radiative Mid-Range Energy Transfer," *Annals of Physics*, Vol. 323, No. 1, pp. 34-48, January 2008.
[7] A. R. Silva and M. C. Vuran, "Development of a Testbed for Wireless Underground Sensor Networks," *EURASIP Journal on Wireless Communications and Networking (JWCN)*, vol. 2010, Article ID 620307, doi:10.1155/2010/620307.
[8] Z. Sun and I. F. Akyildiz, "Connectivity in Wireless Underground Sensor Networks," in *Proc. IEEE SECON '10*, Boston, USA, June 2010.
[9] M.C.K. Wiltshire, E. Shamonina, I.R. Young and L. Solymar, "Dispersion characteristics of magneto-inductive waves: comparison between theory and experiment," *Electronics Letters*, vol. 39, no. 2, pp. 215-217, 2003.
[10] Z. Sun and I. F. Akyildiz, "Deployment Algorithms for Wireless Underground Sensor Networks using Magnetic Induction," in *Proc. IEEE Globecom'10*, Miami, USA, December 2010.
[11] P. Gupta and P. R. Kumar, "The Capacity of Wireless Networks," *IEEE Transactions on Information Theory*, vol. 46, no. 2, pp. 388-404, March 2000.
[12] C. X. Wang, X. Hong, H. H. Chen, and J. Thompson, "On Capacity of Cognitive Radio Networks with Average Interference," *IEEE Transactions on Wireless Communications*, vol. 8, no. 4, pp. 1536-1276, April 2009.
[13] V. Bhandari and N. H. Vaidya, "Capacity of Multi-Channel Wireless Networks with Random (c, f) Assignment," in *Proc. ACM MobiHoc'07*, New York, USA, September 2007.
[14] B. Liu, Z. Liu, D. Towsley, "Capacity of a Wireless Ad Hoc Network with Infrastructure," in *Proc. ACM MobiHoc'07*, New York, USA, September 2007.
[15] C. Jiang, Y. Shi, Y.T. Hou, and S. Kompella, "On the Asymptotic Capacity of Multi-Hop MIMO Ad Hoc Networks," *IEEE Transactions on Wireless Communications*, vol. 10, no. 4, pp. 1032-1037, April 2011.
[16] A. Spyropoulos and C. S. Raghavendra, "Capacity Bounds For Ad-Hoc Networks Using Directional Antennas," in *Proc. IEEE ICC'03*, Anchorage, USA, May 2003.